P8.1   OBSERVING CLEAR AIR TURBULENCE INDIRECTLY IN SATELLITE IMAGERY

Anthony Wimmers*, Wayne Feltz

University of Wisconsin – Cooperative Institute for Meteorological Satellite Studies

1. OBJECTIVE

To resolve areas of clear air turbulence in near-real time over the United States using a GOES derived product that predicts tropopause folding at air mass boundaries.

2. INTRODUCTION

The True Water Vapor (TWV) product is a derived product image, based on the GOES water vapor channel, depicting specific humidity at a fixed layer in the upper troposphere (250-500 hPa) (Wimmers and Moody, 2001). Recent investigation has found that strong gradients in the image-derived specific humidity correspond closely with tropopause folding (Wimmers and Moody, 2004a, 2004b), described as an event in which the boundary between the stratosphere and the troposphere folds into the troposphere, frequently leading to dynamical instability (enhanced turbulence) (Shapiro, 1980) and chemical mixing between the two regions.

This paper describes an empirical model of tropopause folding based on the TWV product that is used to predict areas of clear air turbulence. An ongoing validation of this Tropopause Folding Product (TFP) uses pilot reports of turbulence received from the Aviation Digital Data Service (ADDS) of the National Weather Service Aviation Weather Center and automated commercial aircraft records of high-resolution eddy dissipation rate (EDR) (Cornman et al., 2004) obtained from NCAR.

3. TROPOPAUSE FOLDING MODEL

Recently, Wimmers and Moody (2004a) determined a threshold that distinguishes TWV image gradients strong enough to correspond to tropopause folds, and predicted folds in 13 out of 14 cases, with no false

_____

* *Corresponding author address*: Anthony Wimmers, UW-CIMSS, 1225 W. Dayton St., Madison, WI 53706 wimmers@ssec.wisc.edu

positives. However, the gradient magnitude does not go further to predict the size of the tropopause folds (Wimmers and Moody, 2004b). Consequently, the resulting empirical model for estimating tropopause folding uses an "average" tropopause folding size, which was found to be without significant bias over latitude or gradient magnitude.

Tropopause folds are modeled as "ribbons" of uniform width (234 km), with one edge along the gradient maximum (shown in the images as the darker edge), indicating the opening of the tropopause fold. The other edge extends out in the direction of higher moisture, modeling a fold oriented toward and underneath the warmer air mass. Fold height is estimated by taking the height of the tropopause at the "opening" of the tropopause fold, and extending this layer isentropically according to the 3-D temperature fields of the corresponding RUC-2 model. The layer thickness extends from 5K below this height to 15K above.

4. VALIDATION METHOD

The Tropopause Folding Product was validated with an eight-month record of GOES-12 imagery and pilot reports from September 2004 to April 2005 and a four-month record of imagery and automated eddy diffusion rate data from November 2004 to February 2005. Only data east of 100W longitude was used (in order to eliminate mountain wave turbulence from the Rockies), and a primitive cloud mask (all points >210K) was used to reduce the incidence of turbulence due to convection. To test only for the heights sensitive to tropopause folding, all validation data was limited to altitudes of 5,000 meters and above.

Model skill is measured by the fraction of "turbulent" reports to total observations within the modeled tropopause folds. If the fraction is higher than the fraction attributable to the "background" level (the total fraction of the dataset) then the model is said to have skill. In the dataset of manual pilot reports, turbulence is defined as a rating above 0 (on a scale of 0 to 8). In the

automated EDR dataset, turbulence is defined as $\varepsilon^{2/3} > 0.05$.

5. RESULTS AND DISCUSSION

a. Pilot report validation

Plotting results with time (Figure 1) reveals that the model only shows skill between November and February. During this time of year, baroclinicity in the midlatitudes is the greatest, and so one would expect a gradient-based tropopause folding model to represent more intense tropopause folds than in the other months. Because of this result, the data in the following analyses was trimmed to the November 2004 to February 2005 time period.

When organized by "fold orientation" (Figure 2), the lowest accuracy occurs when the tropopause fold is oriented to the south, and the highest accuracy is when the fold is oriented to the northeast. This could be because U.S. aircraft experience less turbulence when flying along the jet stream than when crossing it, and suggests a sensitivity in the results to the east-west bias of the air traffic corridors.

When organized by distance from the tropopause break (Figure 3), accuracy is apparently lowest within 22 km from the tropopause break, and consistently high from this distance to the end of the modeled folding length. This indicates a spatial error in the pilot reports; that is, the reported events may be just outside the tropopause break if they are reported to be near the break. Otherwise, accuracy is high throughout the distance from the tropopause break.

Sorting the data by image gradient magnitude (Figure 4), it can be seen that the accuracy does not increase with the intensity of the image gradient associated with the tropopause fold. This could be because pilots avoid the strongest events, or because the model is tuned to lower gradients.

Finally, the data is sorted by height with respect to the center potential temperature of the tropopause fold (Figure 5). In the figure, accuracy peaks in the center height, and decreases slightly with distance from the center. These results confirm that the model is well-tuned to the height of the modeled tropopause folds.

b. EDR validation

The main difference between pilot report and EDR data is that turbulence occurs much less frequently in the automated EDR results. Because EDR data is nearly continuous during the participating aircraft flights, this dataset shows roughly the frequency of significant turbulence above 5,000 meters, and it also shows the relative bias of turbulence reporting in the pilot report dataset (an average frequency of turbulence of 67% in pilot reports versus 1.3% in automated EDR reports). In the following discussion, it is important to note that a turbulence-generating tropopause fold will generate a positive observation only sporadically through the fold, and that the fraction of turbulence observations would be much higher in manual reports than in automated reports, because the manual reports would integrate the experience of turbulence into one comprehensive observation. Thus, a frequency of observed turbulence on the order of 5% is highly significant in an EDR dataset, but it would be trivial in a pilot report dataset.

When plotting frequency of turbulence with compass direction from fold (Figure 6), the results are generally consistent with pilot reports: accuracy is the greatest when the orientation is to the east, and weakest when the orientation is generally to the south.

Results are also similar for turbulence frequency versus distance from tropopause break (Figure 7): accuracy is low for areas nearest the tropopause break, probably due to spatial error. However, the accuracy is also low beyond 180 km (1.6 g.c.d.) from the tropopause break. Although this contradicts the pilot report results, the contradiction is probably due to undersampling in the pilot reports.

Also in contrast to the pilot report results, the accuracy was negligible for image gradients below 6 K/g.c.d (Figure 8). But surprisingly, the accuracy peaks at 8 K/g.c.d. and returns to insignificant levels at 10 K/g.c.d. (The accuracy at 14 K/g.c.d. is not discussed because it is undersampled.)

When the data is sorted by height, a result very similar to that of the pilot reports is obtained (Figure 9). The tropopause folding range (-5K to +15K of the central potential temperature) is

validated over most of the range. However, the accuracy is not significant above +10K.

Taken together, these EDR results can be used to guide the development of a more elaborate and more robust model. For instance, the high accuracy of the current model for eastward-facing tropopause folds indicates that the image gradient threshold can be relaxed in these cases. However, the low accuracy for southward-facing tropopause folds (but high sample size) indicates that the image gradient threshold should be increased in these cases.

6. CONCLUSIONS

- The available data shows that the TFP model demonstrates skill at predicting turbulence for modeled folds between November and February.

- Accuracy at predicting turbulence is highly dependent on the orientation of the tropopause fold, which might, in turn, bias the observations because of aircraft direction and flight track.

- Pilot reports and EDR data are in general agreement, with the only significant contrasts occurring where pilot report data is undersampled.

- The data show that improvements to the model can be made by 1) Truncating the modeled folding width to 180 km, 2) Shortening the fold "height" from +15 K to +10 K above the central potential temperature, and 3) Developing an optimal relationship between tropopause fold orientation and threshold gradient magnitude.

- We are currently working with NCAR to combine this model with the NCAR ADDS model to provide a finer-scale clear-air turbulence component to the general flight hazard model.

7. REFERENCES

Cornman, L. B., P. Schaffner, C. A. Grainger, R. T. Neece, T. S. Daniels and J. J. Murray, (2004) Eddy dissipation rate performance of the Tropospheric Airborne Meteorological Data Reporting (TAMDAR) sensor during the 2003 Atlantic THORPEX regional campaign, 11th conference on aviation, range and aerospace, American Meteorological Society, 4-9 October 2004.

Shapiro, M.A., (1980) Turbulent mixing within tropopause folds as a mechanism for the exchange of chemical constituents between the stratosphere and troposphere, J. Atmos. Sci., 37, 994-1004.

Wimmers, A.J., and J.L. Moody, (2001) A fixed-layer estimation of upper tropospheric specific humidity from the GOES water vapor channel: Parameterization and validation of the altered brightness temperature product, *J. Geophys. Res.*, *106* (D15), 17115-17132.

Wimmers, A. J., and J. L. Moody (2004), Tropopause folding at satellite-observed spatial gradients: 1. Verification of an empirical relationship, J. Geophys. Res., 109, D19306, doi:10.1029/2003JD004145.

Wimmers, A. J., and J. L. Moody (2004), Tropopause folding at satellite-observed spatial gradients: 2. Development of an empirical model, J. Geophys. Res., 109, D19307, doi:10.1029/2003JD004146.

Acknowledgments
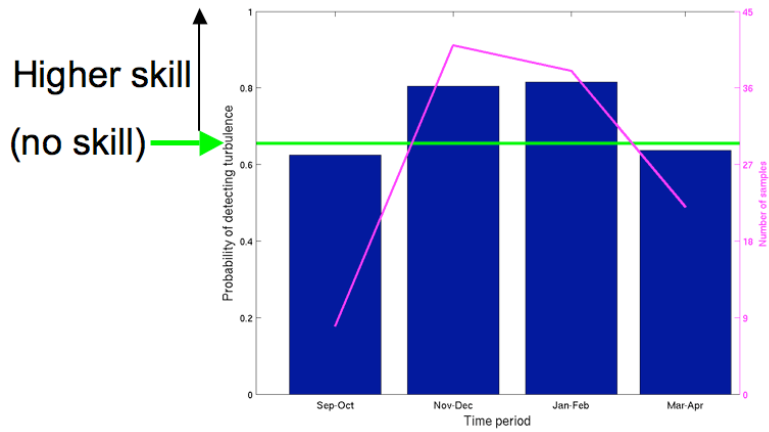
Figure 1. Accuracy of tropopause folding model as a function of time, validated by pilot reports of turbulence; blue bar, probability of detecting turbulence; green line, overall frequency of turbulence in pilot reports; pink line, number of samples (right axis).
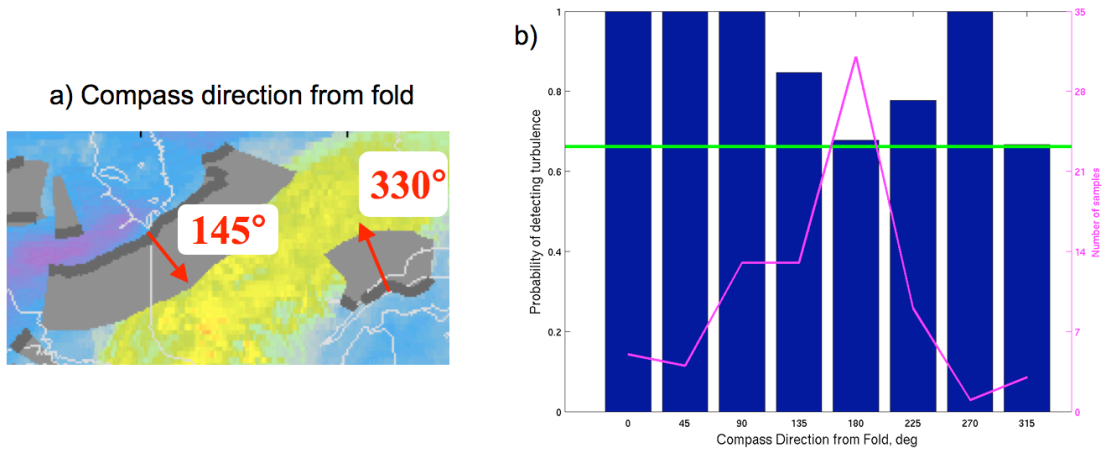
Figure 2. a) Example of modeled tropopause folds and compass direction of the folds validated by pilot reports of turbulence, b) Accuracy of tropopause folding model as a function of compass direction, validated by pilot reports of turbulence; green line, overall frequency of turbulence in pilot reports; pink line, number of samples (right axis).

a) Distance from tropopause break

1 g.c.d.

2 g.c.d.

b)
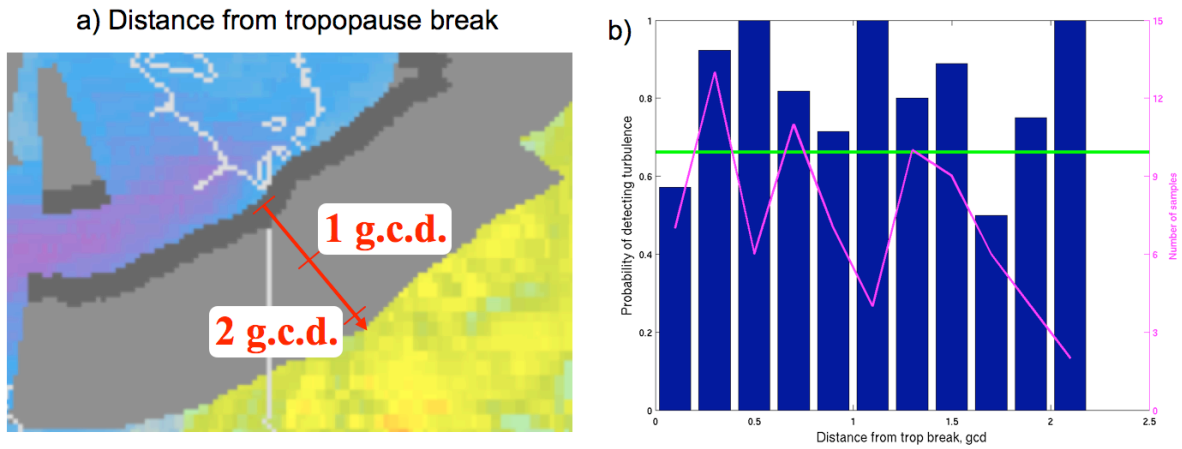
Figure 3. Example of modeled tropopause folds and distance from tropopause break, b) Accuracy of tropopause folding model as a function of distance from tropopause break, validated by pilot reports of turbulence; green line, overall frequency of turbulence in pilot reports; pink line, number of samples (right axis).
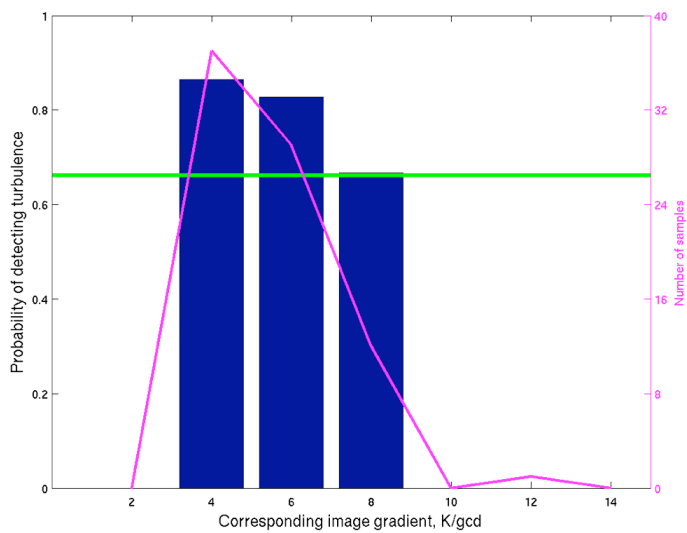
Figure 4. Accuracy of tropopause folding model as a function of corresponding image gradient, validated by pilot reports of turbulence; green line, overall frequency of turbulence in pilot reports; pink line, number of samples (right axis).
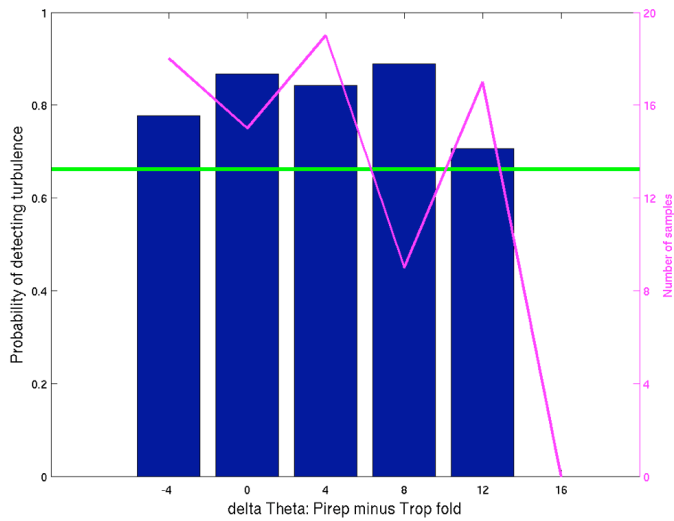
Figure 5. Accuracy of tropopause folding model as a function of potential temperature difference between observations and the modeled tropopause fold, validated by pilot reports of turbulence; green line, overall frequency of turbulence in pilot reports; pink line, number of samples (right axis).
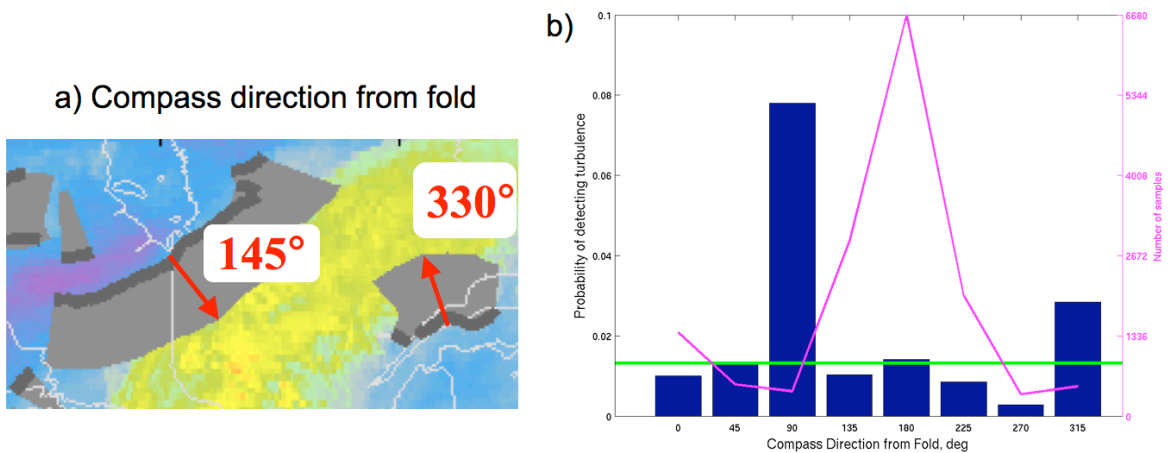
Figure 6. a) Example of modeled tropopause folds and compass direction of the folds validated by automated EDR data, b) Accuracy of tropopause folding model as a function of compass direction, validated by pilot reports of turbulence; green line, overall frequency of turbulence in pilot reports; pink line, number of samples (right axis).

a) Distance from tropopause break
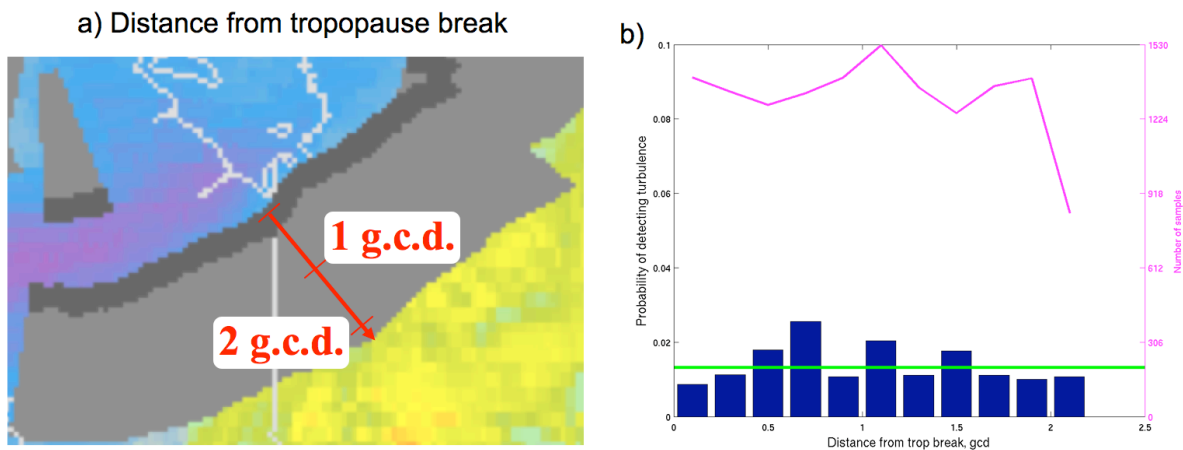
Figure 7. Example of modeled tropopause folds and distance from tropopause break, b) Accuracy of tropopause folding model as a function of distance from tropopause break, validated by automated EDR data; green line, overall frequency of turbulence in pilot reports; pink line, number of samples (right axis).
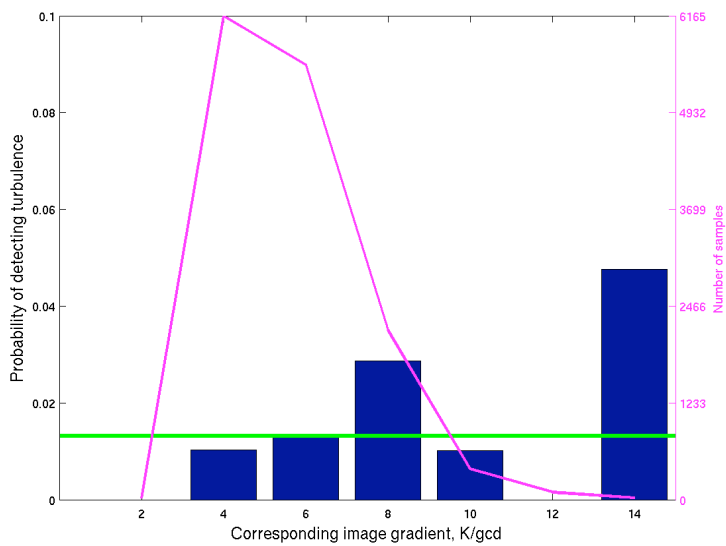
Figure 8. Accuracy of tropopause folding model as a function of corresponding image gradient, validated by automated EDR data; green line, overall frequency of turbulence in pilot reports; pink line, number of samples (right axis).
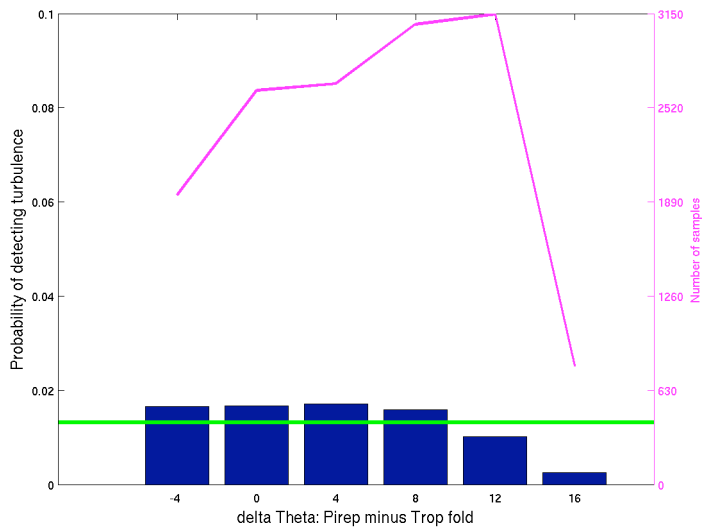
Figure 9. Accuracy of tropopause folding model as a function of potential temperature difference between observations and the modeled tropopause fold, validated automated EDR data; green line, overall frequency of turbulence in pilot reports; pink line, number of samples (right axis).